Available online at www.sciencedirect.com

ScienceDirect

Ceramics International 40 (2014) 3221–3226

CERAMICS INTERNATIONAL

www.elsevier.com/locate/ceramint

Large-area TiO_2 nanotube dye-sensitized solar cells using thermal-sprayed Ti layers on stainless steel

Chien Chon Chen[a], Wern-Dare Jheng[b,*], Chung-Kwei Lin[c,*]

[a]Department of Energy Engineering, National United University, Miaoli 36003, Taiwan
[b]Department of Mechanical Engineering, National Chin-Yi University of Technology, Taichung 411, Taiwan
[c]School of Dental Technology, College of Oral Medicine, Taipei Medical University, Taipei 11031, Taiwan

Received 1 September 2013; received in revised form 25 September 2013; accepted 25 September 2013
Available online 3 October 2013

Abstract

This work presents large-scale dye-sensitized solar cells and methods for their manufacture. A dye-sensitized solar cell device contains a photosensitive dye adsorbed on a large surface of the anode, and a transparent conductive cathode disposed opposite the anode, wherein platinum nano-catalytic particles adhere to its surface, and an electrolytic solution is sealed between the anode and the transparent conductive cathode. A titania nanotube film was fabricated by thermo-spraying titanium film on 304 stainless-steel substrate. The photo-current conversion efficiency was tested under an AM 1.5 solar simulator. The dye-sensitized solar cell device has a short current density of 8.22 mA cm^{-2}, open voltage of 0.71 V, fill factor of 0.59, and conversion efficiency of 3.4%. The internal impedance of the dye-sensitized solar cell was detected and simulated using an electrical impedance spectra technique with inductance, resistance, and capacitance characteristics. The stainless-steel/titania, titania/electrolyte, electrolyte, and electrolyte/(platinum/indium tin oxide) interfaces were simulated using an resistor–capacitor parallel circuit, and bulk materials such as stainless steel, tin doped indium oxide, and conducting wire were simulated by using a series of resistors and inductance.

Keywords: Dye-sensitized solar cell; Stainless-steel; Efficiency; Electrochemical impedance spectroscopy; Equivalent circuit

1. Introduction

A typical dye-sensitized solar cells (DSSCs) device contains a light-harvesting layer on a working electrode (anode) and a Pt-coated layer on a counter-electrode (cathode); both electrodes are made of a transparent conducting oxide (TCO) substrate [1–4]. The first TiO_2 nanotube arrays were made by Zwilling et al. [5], and these arrays were studied in greater detail recently by Cai et al. [6] and Grimes [7]. These groups fabricated TiO_2 nanotubes (NT) by anodization, and the length of the tubes was controlled by varying the amount of fluoride ions in the electrolyte [8]. For example, an aqueous HF-based electrolyte enabled 0.5 μm long nanotubes, an aqueous NaF or KF-based electrolyte enabled 6.8 μm long nanotubes [7], and a nonaqueous F ion-based electrolyte enabled 134 μm nanotubes [9]. Varghese et al. [10] discussed the fabrication of thick nanotube array films on fluorine doped tin oxide (FTO) film but used sputtering (a very slow process) to deposit the Ti layer from which the nanotubes formed. In Gopal's [11] research, a dye sensitized solar cell (DSSC) anode of 0.36 μm length was formed on FTO glass and had a photocurrent efficiency of 2.9% under an AM 1.5 solar simulator.

In principle, electrochemical impedance spectroscopy (EIS) measurements cover a broad frequency range, and they may provide information on the interfaces of electron transport and charge transfer characterizations [12–14]. An analysis of the DSSC describing electron transport and charge recombination in nanoparticles and nanotube films has been presented based on the transmission line model [15–18]. Kern et al. [19] indicated that in the Nyquist plot, the low-frequency range corresponds to the electrolyte, the middle-frequency range reflects the anode, and the high-frequency range corresponds to the cathode. Hoshikawa et al. [20] also reported that the semicircles of ω_1, ω_2, ω_3, and ω_4 were attributed to the electron transfer at the transparent conduction oxide (TCO)/TiO_2

*Corresponding authors.
E-mail addresses: jwd@ncut.edu.tw (W.-D. Jheng), chungkwei@tmu.edu.tw (C.-K. Lin).

0272-8842/$ - see front matter © 2013 Elsevier Ltd and Techna Group S.r.l. All rights reserved.
http://dx.doi.org/10.1016/j.ceramint.2013.09.116

interface, in TiO_2 particles, and at the TiO_2/I_3^- interface, and the diffusion impedance of I_3^- in the electrolyte, respectively. Zhu et al. [21] found that the DSSC conversion efficiency was in direct proportion to TiO_2 length. When TiO_2 nanotubes were formed on Ti foil by anodization with lengths of 1.9–5.7 μm, the photocurrent efficiency was from 1.7% to 3%. According to Smestad's [22] report, DSSCs are made from inexpensive materials and are easier to fabricate than amorphous silicon solar cells. However, the expensive conductive materials (ITO, ATO, or FTO) [23,24] raise the cost of DSSCs, and a complex process is required to coat TiO_2 particles on the conductive materials. In our work, the DSSC anodes of FTO and TiO_2 particles were replaced with sprayed Ti and TiO_2 nanotubes. The ability to spray on the Ti could change the entire field of short TiO_2 NT and expensive FTO issues. We also report and analyze the characteristics of DSSCs made by spraying on the Ti film. Electrical impedance spectra are used to describe the ohmic resistance, electron transfer resistance, diffusion resistance, charge-transfer resistance, contact capacitance, chemical capacitance, electrolysis capacitance, double-layer capacitance, ohmic inductance, and inductive inductance in NT TiO_2 DSSC under simulated AM 1.5 light intensity.

2. Experimental

A 304 stainless-steel (S.S.) plate with a size of 10 cm × 10 cm × 1 cm was used as the DSSC anode substrate. The substrate was first sandblasted with a free-stream velocity of 5–20 m/s and Al_2O_3 particles of 10–15 μm. Titanium film of 50–100 μm thickness was deposited on the 304 S.S. using Ti powder (50 μm particle size) and coated by a high velocity oxygen fuel (HVOF) thermal spray method. The input fuel of HVOF was a mixture of oxygen (10 MPa), hydrogen (0.3 MPa), and air (0.3 MPa). The flame speed was about 2000 m/s, and flame temperature was about 270 °C. The spraying distance was kept constant at 10 cm perpendicular to the sample surface. The Ti film was then treated with anodization, $TiCl_4$ treatment, and heat treatment to form anatase TiO_2 NT film, which was the anode of the DSSC.

TiO_2 NT growth was achieved using an electrolyte (pH=6.8) of 0.5 wt% ammonium fluoride (NH_4F, 99.9%) and 2 wt% H_2O in ethylene glycol ($C_2H_4(OH)_2$) solvent with applied 1 h potentiostat (60 V) and 1 h galvanostat anodization (4.44 mA cm^{-2}) for various periods of anodization. Any substrate not covered by TiO_2 NT film was treated with titanium tetrafluoride (TiF_4). After TiO_2 NT samples were formed by anodization and TF_4 treatment, the samples were then annealed in an air furnace at 450 °C for 1 h to form anatase phase TiO_2 NT film. The DSSC anode was thus formed. An indium doped tin oxide (ITO) glass coated with platinum (Pt) particles by sputtering was used as a counter-electrode. Electrolyte containing 0.5 M lithium iodide (LiI) and 0.05 M iodine (I_2) in acetonitrile (CH_3CN, 99.9%) was introduced into the electrodes. To fabricate the NT-DSSC device, we assembled the two electrodes into a sandwich-type cell and sealed it with a hot-melt film (SX1170, Solaronix, thickness 25 μm).

The N3 dye absorbed by the TiO_2 NT was measured using UV–visible–NIR spectrophotometers at room temperature. The EIS measurements were carried out with the impedance measuring unit (IM 6) from Zahner. Electrochemical measurements were carried out in a two-electrode configuration, with the Pt/ITO electrode as the counter-electrode and dye/TiO_2 NT/ 304 S.S. as the working-electrode. Measurements of the impedance of the cells were recorded over a frequency range of 3×10^{-3}–4×10^{6} Hz with an ac amplitude of 10 mV under various intensities of the AM 1.5 solar simulator. The EIS data were analyzed by the equivalent circuit mold and fitted.

3. Results and discussion

Fig. 1 shows a schematic diagram of the DSSC device fabricated with 304 S.S. substrate and TiO_2 NT. The structure includes ITO glass, a counter-electrode of Pt particles, electrolyte, and a working electrode of 304 S.S. substrate, TiO_2 NT, and dye. After DSSC irradiation by incident light, the electrons of the photosensitive dye are excited from the ground state to the excited state. (i) The electrons are transferred from the excited state of the photosensitive dye molecules (N3) to a conductive band of the semiconductor layer (TiO_2 NT). The electrolytic solution ($LiI+I_2$) is simultaneously oxidized, and the photosensitive dye is reduced. This process corresponds to holes transfer from photosensitive dye molecules to an electrolytic solution. (ii) The electrons in the semiconductor layer are then transferred from a conductive layer (304 S.S.) to an external circuit and do work on external loads. (iii) The electrons return to the electrolytic solution from the external circuit via the cathode (ITO) and reduce the electrolytic solution.

Fig. 2 shows optical microscopy (OM) images of a dye-sensitized solar cell (DSSC) electrode produced by

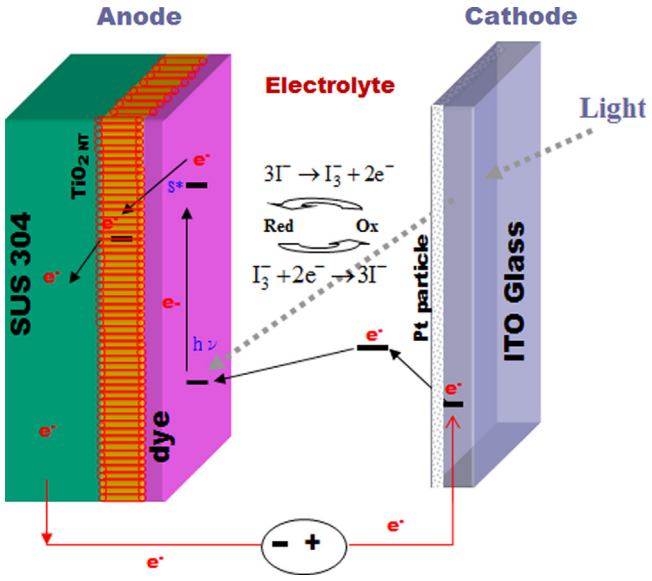

Fig. 1. Schematic diagram of DSSC device fabricated with 304 S.S. substrate and TiO_2 NT. The structure consists of ITO glass, a counter-electrode of Pt particles, electrolyte, and a working electrode of 304 S.S. substrate, TiO_2 NT, and dye.

thermo-spraying, anodization, and heat treatment processes. Ti film was deposited on 304 stainless steel by thermo-spraying to get Ti film (50–100 μm) on 304 S.S. substrate. Porous Ti film was modified by TiF_4 solution so that $Ti(OH)_4$ could be formed in the pores, increasing the TiO_2 NT active surface area and forming a barrier against current leakage between the 304 S.S. and dye. After heat treatment at 450 °C for 1 h, amorphous phase TiO_2 NT $Ti(OH)_4$ and amorphous phase TiO_2 NT can transform into anatase TiO_2 NT. Therefore, a large area DSSC anode was formed from anatase, a semiconductor of anatase TiO_2 NT, and metal substrate of 304 S.S. Fig. 3 shows SEM images of TiO_2 NT film formed by anodization on thermo-sprayed Ti film. The TiO_2 NT was produced with hybrid anodization of 1 h potentiostat (60 V) and 1 h galvanostat anodization (4.44 mA cm^{-2}). This figure shows (a) the surface morphology of titanium thermal sprayed film, consisting of plane film, Ti drops, and Ti particle surfaces formation TiO_2 NT, (b) TiO_2 NT formed on the plane film, and (c) enlarged view of plane film surface. According to SEM images, TiO_2 NT has ordered pores with a diameter of 100 nm, pore distance of 140 nm, pore wall thickness of 20 nm, and density of 5×10^9 pore cm^{-2}.

Fig. 4 shows the absorbance and photocurrent density–voltage (J–V) properties of TiO_2 NT on N3 dye and DSSC under simulated AM 1.5 light. Fig. 4(a) shows that the N3 dye absorbance ranges from 350 nm to 800 nm, and two absorbance peaks of 410 nm and 535 nm are present at the absorbance curve. Fig. 4(b) shows that the DSSC device has a short current density (Jsc) of 8.22 mA cm^{-2}, an open voltage (Voc) of 0.71 V, a fill factor (FF) of 0.59, and conversion efficiency (η) of 3.4%. The internal impedance on the DSSC interfaces could also be detected, and detailed analysis was performed by EIS technique. Fig. 5 shows Bode plots of DSSC under various AM 1.5 light intensities. In Fig. 5(a), three regions, $10^{-2.7}$–10^0 Hz, 10^0–10^4 Hz, and 10^4–10^6 Hz, can be discriminated. The regions reflect the impedances of electrolyte, anode, and cathode in the DSSC. Fig. 5(b) indicates that in the Nyquist plot, the low-frequency range corresponds to the electrolyte, while the middle-frequency range reflects the anode, and the high-frequency range corresponds to the cathode. Also, the semicircles of ω_1, ω_2, ω_3, and ω_4 are attributed to the electron transfer at the transparent conduction oxide (TCO)/TiO_2 interface, in TiO_2 particles, at the TiO_2/I_3^- interface, and the diffusion impedance of I_3^- in the electrolyte, respectively.

Fig. 6(a) shows a schematic diagram of the impedance structure of the DSSC. The internal impedances consist of at least twelve electrical components. The internal resistances of electrodes or load wire were simulated by resistance, and the characterization of electron and charge transportation or diffusion between interfaces was simulated by an RC parallel circuit. It was found that the resistances of 304 S.S. substrate (R_0), transport wire, and counter-material (R_b), and a series of inductances (L_0) appeared as ohmic impedance. The ohmic impedance value was independent of lighting intensity. The other resistances, namely TiO_2 resistance (R_a), contact resistance (R_1), diffusion resistance (R_3), and charge-transfer resistance (R_2 and R_4), as the internal resistances, were affected by lighting intensity and determine the performance of the DSSC. The interface capacitances of contact capacitance (C_1), chemical capacitance (C_2), diffusion capacitance (C_3), and double-layer capacitance (C_4) determine the performance of charge transportation on the DSSC interfaces. The ohmic inductance (L_0) expresses the inductance in the loading wire, which was present at the higher frequency point. The equivalent circuit of DSSC can be illustrated as Fig. 6(b), and the equivalent impedance can be expressed as $(L_0+R_0+R_b)+\{[(C_1//R_1)//(R_a+(C_2//R_2))]\}+(C_3//R_3)+(C_4//R_4)$. In the equivalent circuit, the $L_0+R_0+R_b$ impedance was detected in a high frequency range, and the $L_0+R_0+(R_1//R_a)+R_2+R_3+R_4+R_b$ impedance was detected on the real axis at lower frequencies. But the capacitances of C_1, C_2, C_3, and C_4 values were detected on the real and

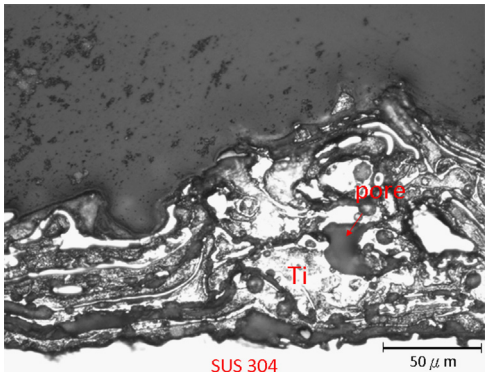

Fig. 2. Optical microscopy (OM) images of dye-sensitized solar cell (DSSC) electrode formed by thermo-spraying Ti film on the 304 stain steel substrate.

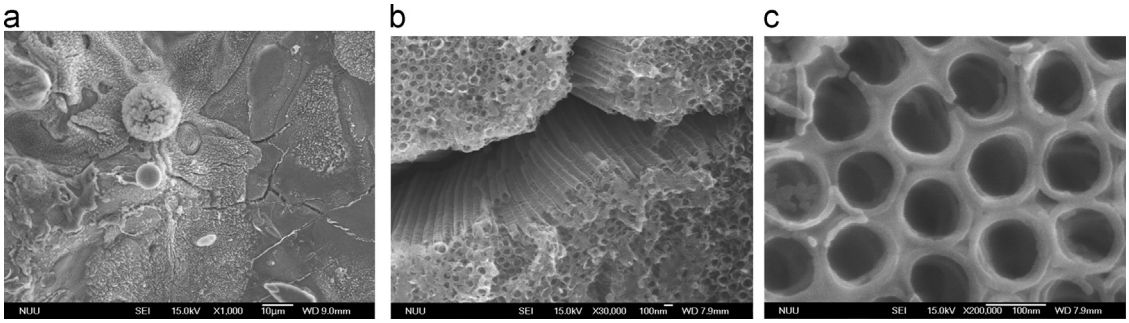

Fig. 3. SEM images of TiO_2 NT film by anodization on thermo-sprayed Ti film; (a) plane film, drop, and particle surface formation of TiO_2 NT, (b) TiO_2 NT formation on the plane film, and (c) enlarged view of plane film surface.

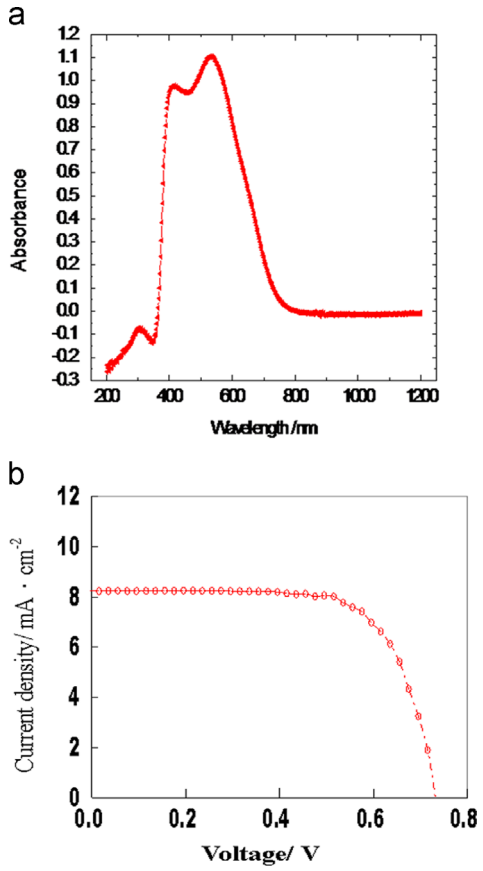

Fig. 4. The DSSC cell performances: (a) absorption spectrum and (b) current density–voltage (*J–V*) curve of photocurrent efficiency.

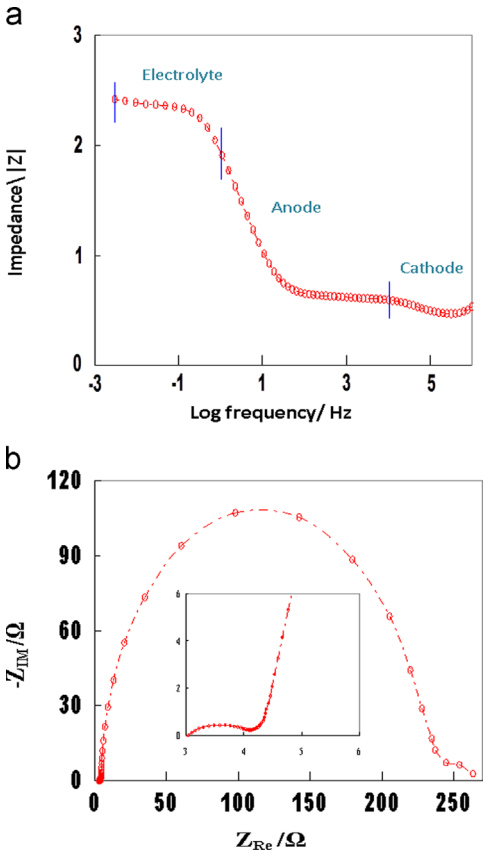

Fig. 5. Bode plot and Nyquist of TiO_2 NT DSSC under AM 1.5 light.

imaginary axes in the middle frequencies. Because the counter of $R_3//C_3$ has lower impedance, the electrolyte of $R_3//C_3$ has higher Warburg diffusion impedance, and the anode of $(C_1//R_1)//(R_a+(C_2//R_2))$ has middle impedance. The semicircles of counter-electrode, anode, and electrolyte are ordered on the Nyquist plot from higher to lower frequencies. Based on EIS data and the equivalent circuit model, the fitting results showed ohmic inductance (L_0, 0.34 μH), ohmic resistance (R_0, 0.3 Ω), and counter-resistance (R_b, 2.6 Ω); the photo-excitation semiconductor property (R_a, 3.2 Ω) of the TiO_2 film; the Ti/TiO_2 interface electron and charge transfer rate (R_1, 0.6 Ω and C_1, 1.8 μF); the TiO_2 electrolyte interface electron and charge transfer rate (R_2, 13 Ω and C_2, 56 μF); oxidation of $3I^- \overset{oxidation}{\rightarrow} I_3^- + 2e^-$ close to the working electrode side and reduction of $I_3^- + 2e^- \overset{reduction}{\rightarrow} 3I^-$ close to the counter-electrode side, such that I_3^- and I^- ions get absorbed on the working and counter-surfaces; and the electrolyte capacitance (C_3, 1803 μF) and the electrolyte resistance (R_3, 215 Ω). The electrolyte/counter-interface has a large quantity charge of I_3^- (C_4, 2.8 μF) and the waiting electron, which on the counter-surface moves and combines with I_3^- (R_4, 0.8 Ω).

4. Conclusions

A large-area DSSC anode was made by thermo-spraying Ti on 304 S.S. substrate and anodization to form TiO_2 NT as an electron transport film, and the performance of the device was measured at 3.4% conversion efficiency. The fabrication process of thermo-spraying and anodization for industry-scale oxide film production is novel. This work aims to transfer nanotechnology discoveries from the laboratory to industrial applications and to scale up DSSC fabrication for high-rate production. The electron and hole transport mechanism was explained by EIS test. The impedance spectra of the TiO_2 NT DSSC showed an internal resistance that consisted of 12 components. The resistances of 304 S.S. (R_0), transport wire and counter-material (R_b), and a series of inductance (L_0) appeared as ohmic impedance. The ohmic impedance value was not affected by sun intensity. The other resistances of TiO_2 resistance (R_a), contact resistance (R_1), diffusion resistance (R_3), and charge-transfer resistance (R_2 and R_4), as the internal resistances, were affected by lighting intensity, and determine the performance of the DSSC. The interface capacitances of contact capacitance (C_1), chemical capacitance (C_2), diffusion capacitance (C_3), and double-layer capacitance (C_4) are determinative in the performance of charge transportation on the DSSC interface. A detailed study of DSSC conversion efficiency under various AM 1.5 lights will be described in a future paper.

Acknowledgments

This study was supported by grants from the National Science Council, Taiwan, under Contracts NSC 101-2627-M-239-001 and NSC 102-2221-E-239-008.

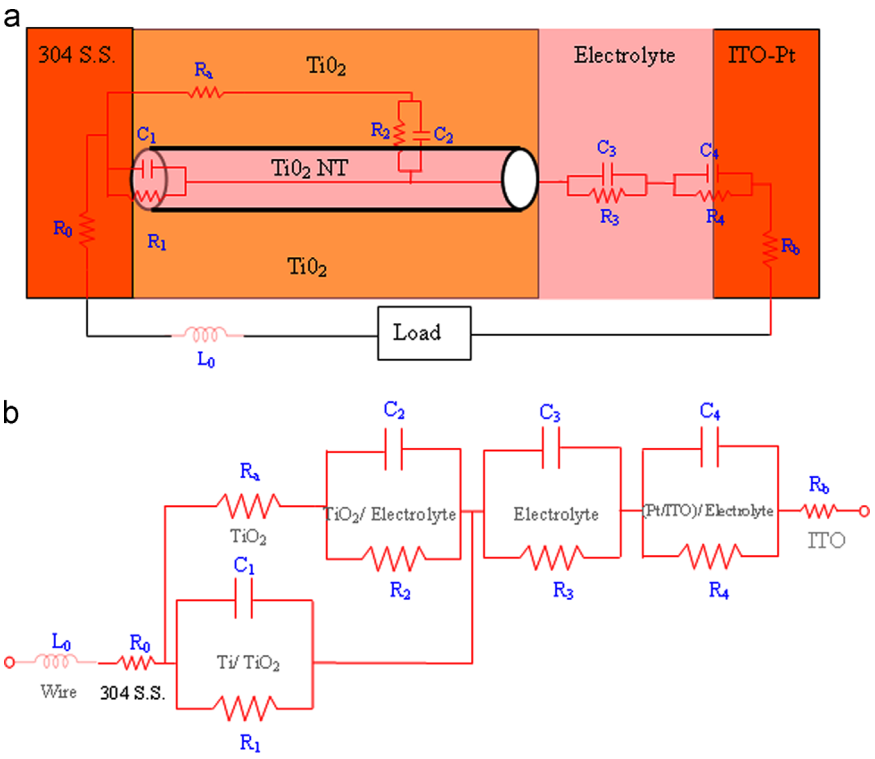

Fig. 6. Schematic diagram of (a) DSSC structure, which can be simulated by using a resistor, capacitor, and inductance. Each individual interface of Pt/ITO – electrolyte, electrolyte – TiO_2, and TiO_2–304 S.S. can be simulated by an RC parallel circuit; the bulk materials of Pt/ITO, Ti, and conducting wire can be simulated by a series of resistors and inductance and (b) equivalent circuit used for modeling the EIS of DSSC. The impedance of the bulk is a simulated series by $L_0+R_0+R_b$, the impedance of the anode is simulated by $(C_1//R_1)//(R_a+(C_2//R_2))$, the electrolyte is simulated by $C_3//R_3$, and the cathode is simulated by $C_4//R_4$.

References

[1] Y. Yang, J. Tao, X. Jin, Q. Qin, New microporous polymer electrolyte based on polysiloxane grafted with imidazolium iodide moieties for DSSC, International Journal of Photoenergy 405738 (2011) 9.

[2] C.H. Chien, M.L. Tsai, C.C. Hsieh, Y.H. Li, Enhanced light harvesting in dye-sensitized solar cell using external lightguide, International Journal of Photoenergy 261828 (2011) 6.

[3] M.S. Liang, C.C. Khaw, C.C. Liu, S.P. Chin, J. Wang, H. Li, Synthesis and characterisation of thin-film TiO_2 dye-sensitised solar cell, Ceramics International 39 (2013) 1519–1523.

[4] A.M. Bakhshayesh, M.R. Mohammadi, The improvement of electron transport rate of TiO_2 dye-sensitized solar cells using mixed nanostructures with different phase compositions, Ceramics International 39 (2013) 7343–7353.

[5] V. Zwilling, M. Aucouturier, E.D. Ceretti, Anodic oxidation of titanium and TA6V alloy in chromic media. An electrochemical approach, Electrochimica Acta 45 (1999) 921–929.

[6] Q. Cai, M. Paulose, O.K. Varghese, C.A. Grimes, The effect of electrolyte composition on the fabrication of self-organized titanium oxide nanotube arrays by anodic oxidation, Journal of Material Research 20 (2005) 230–236.

[7] C.A. Grimes, Synthesis and application of highly ordered arrays of TiO_2 nanotubes, Journal of Materials Chemistry 17 (2007) 1451–1457.

[8] C.C. Chen, D. Fang, Z. Luo, Fabrication and characterization of highly-ordered valve-metal oxide nanotubes and their derivative nanostructures, Reviews in Nanoscience and Nanotechnology 1 (2012) 229–256.

[9] M. Paulose, K. Shankar, S. Yoriya, H.E. Prakasam, O.K. Varghese, G.K. Mor, T.A. Latempa, Anodic growth of highly ordered TiO_2 nanotube arrays to 134 μm in length, Journal of Physical Chemistry B 110 (2006) 16179–16184.

[10] Oomman K. Varghese, Maggie Paulose, Craig A. Grimes, Long vertically aligned titania nanotubes on transparent conducting oxide for highly efficient solar cells, Nature Nanotechnology 4 (2009) 592–597.

[11] G.K. Mor, K. Shankar, M. Paulose, O.K. Varghese, C.A. Grimes, Use of highly-ordered TiO_2 nanotube arrays in dye-sensitized solar cells, Nano Letters 6 (2006) 215–218.

[12] H. Hasannejad, T. Shahrabi, M. Jafarian, A. Sabour Rouhaghdam, EIS study of nano crystalline Ni–cerium oxide coating electrodeposition mechanism, Journal of Alloys and Compounds 509 (2011) 1924–1930.

[13] Waheed A. Badawy, Khaled M. Ismail, Ahlam M. Fathi, The influence of the copper/nickel ratio on the electrochemical behavior of Cu–Ni alloys in acidic sulfate solutions, Journal of Alloys and Compounds 484 (2009) 365–370.

[14] Chokri Khaldi, Hamadi Mathlouthi, Jilani Lamloumi, Electrochemical impedance spectroscopy study of the metal hydride alloy/electrolyte junction, Journal of Alloys and Compounds 479 (2009) 284–289.

[15] L. Andrade, S.M. Zakeeruddin, M.K. Nazeeruddin, H.A. Ribeiro, A. Mendes, M. Gratzel, Influence of sodium cations of N3 dye on the photovoltaic performance and stability of dye-sensitized solar cells, ChemPhysChem 10 (2009) 1117–1124.

[16] J. Bisquert, M. Gratzel, Q. Wang, F.F. Santiago, Three-channel transmission line impedance model for mesoscopic oxide electrodes functionalized with a conductive coating, Journal of Physical Chemistry B 110 (2006) 11284–11290.

[17] G. Franco, J. Gehring, L.M. Peter, E.A. Ponomarev, I. Uhlendorf, Frequency-resolved optical detection of photoinjected electrons in dye-sensitized nanocrystalline photovoltaic cells, Journal of Physical Chemistry B 103 (1999) 692–698.

[18] F.F. Santiago, E.M. Barea, J. Bisquert, G.K. Mor, K. Shankar, C.A. Grimes, High carrier density and capacitance in TiO_2 nanotube arrays induced by electrochemical doping, Journal of the American Chemical Society 130 (2008) 11312–11316.

[19] R. Kern, R. Sastrawan, J. Ferber, R. Stangl, J. Luther, Modeling and interpretation of electrical impedance spectra of dye solar cells operated under open-circuit conditions, Electrochimica Acta 47 (2002) 3225–4213.
[20] T. Hoshikawa, M. Yamada, R. Kikuchi, K. Eguchi, Impedance analysis of internal resistance affecting the photoelectrochemical performance of dye-sensitized solar cells, Journal of the Electrochemical Society 152 (2005) E68–E73.
[21] K. Zhu, N.R. Nwale, A. Miedaner, A.J. Frank, Enhanced charge-collection efficiencies and light scattering in dye-sensitized solar cells using oriented TiO_2 nanotubes arrays, Nano Letters 7 (2007) 69–74.
[22] G. Smestad, C. Bignozzi, R. Argazzi, Testing of dye sensitized TiO_2 solar cells I: experimental photocurrent output and conversion efficiencies, Solar Energy Materials and Solar Cells 32 (1994) 259–272.
[23] B. Stjerna, E. Olsson, C.G. Granqvist, Optical and electrical properties of radio frequency sputtered tin oxide films doped with oxygen vacancies, F, Sb, or Mo, Journal of Applied Physics 76 (1994) 3797–3817.
[24] F.A. Guo, G. Li, W. Zhang, Barium staminate as semiconductor working electrodes for dye-sensitized solar cells, International Journal of Photoenergy 2010 (2010) 105878 (pages 7).